Chemistry and Materials Research
ISSN 2224- 3224 (Print) ISSN 2225- 0956 (Online)
Vol.7 No.7, 2015
www.iiste.org

Corrosion Control of Mg-Zn Implant Alloys in Simulated Body Fluid

I. M. Ghayad*, M. A. Maamoun, W. A. Metwally, A.N.Abd El-Azim, and Z.M. El-Baradie
Central Metallurgical Research and Development Institute (CMRDI),
P.O.Box:87; Helwan, Cairo, Egypt,

This research is financially supported by the Science and Technology Development Fund (STDF), Egypt, Project Grant No. ID: 5342.

Abstract
Magnesium alloys have recently attracted the attention as a new biodegradable material. In this study, Mg-Zn alloys (1-4wt.% Zn) were fabricated with high purity raw materials using a clean melting process (fluxless method) and a protective atmosphere of CO_2 + 0.4 SF_6. The as-cast microstructures of the investigated alloys were characterized by optical and scanning electron microscopes, EDS and XRD. Corrosion properties of the prepared alloys were examined in simulated body fluid (SBF) by electrochemical techniques and immersion test (hydrogen evolution method). Surface modification of the prepared alloys was performed using micro arc oxidation (MAO) treatment and hydroxiapatite (HA) coating.
The results of the as-cast microstructure showed that Zn up to 2 wt% was completely dissolved in α-Mg matrix. On increasing Zn content (> 2wt%) the grain size decreased and a second $MgZn_2$ phase was observed. Corrosion testing results revealed that Mg-1,2,3 wt% Zn have almost the same corrosion rates (0.025 mm/y) whereas Mg-4Zn has the highest degradation rate. Hydroxiapatite (HA) coating on micro-arc oxidation (MAO) treated magnesium alloys formed a dense and compact layer on the surface of magnesium alloys which had greatly improved surface properties and enhanced corrosion resistance of the prepared alloys.
Keywords: Mg alloys, implants, biodegradable, corrosion, surface modification

1. Introduction

In recent years, there has been an increasing interest in magnesium alloys as a biodegradable metal implants in orthopedic surgery, because of its biocompatibility, biodegradability and similar mechanical properties as natural bone [1].

The major limitation of magnesium is its low corrosion resistance which can cause a reduction in the mechanical integrity of the implant before the bone or tissue has sufficiently healed [2]. It also leads to a rapid production of hydrogen gas and the formation of gas bubbles which can accumulate around the implant and delay healing of the tissue [3]. The localized formation of hydrogen gas may also result in a pH increase around the implant and severely affect the pH-dependent physiological process in the vicinity of the implant [1,4]. Therefore a significant, uncontrolled, local change in Mg concentration due to implant degradation must be managed through proper engineering design. Controlling the degradation rate can be attained by modification of the alloy microstructure, alloying Mg with other elements and surface treatment or application of a suitable coating on Mg alloys [5-9].

Studies showed that purification of Mg reduces the corrosion rate considerably; however, due to the low yield strength of pure Mg, its application in orthopedics and other load bearing applications is limited [1].

Alloying elements added to increase the strength of pure Mg should be carefully selected to maintain the Mg's biocompatibility [10] and to reduce toxicity. The effect of alloying elements on the biodegradation behavior of Mg implants material is still unclear [11].

A corrosion resistant coating can significantly improve biodegradation of Mg alloys. Ideally, the corrosion resistant film formed on a magnesium implant should also be wear resistant so that the film will not be damaged by scratching during implanting [1,12].

Based on the above considerations; Zn was selected as an alloying element to develop cast Mg implant alloys with varying Zn content (1-4 wt%). Preparation of these Mg alloys was carried out using fluxless method. Macro and microstructures characterization using optical and scanning electron microscopes was examined. Corrosion behavior of the prepared Mg alloys was thoroughly investigated. The effect of surface treatment on the performance of the prepared alloys was also studied.

2. Experimental Procedure

2.1. Materials and Preparation

Magnesium–Zinc alloys were prepared using pure magnesium (99.9%), pure zinc (99.99%) ingots as a starting materials. Melting and alloying operations were carried out at 750 °C in mild steel crucible using resistance electric furnace under the protection of a gas mixture of CO_2 + 0.4% SF_6. Zn was added in the range 1-4 wt.%. The melt was stirred using mechanical stirrer and was kept after stirring for 10 minute at 750 °C to ensure

complete dissolution of the alloying elements in the melt. The molten metal was skimmed periodically. Finally, the melt was cast into cast iron mold preheated to 250 °C. The chemical compositions of the prepared Mg-Zn lloys were analyzed using Niton XL3t XRF mobile analyzer as shown in Table 1.

2.2. Microstructure Characterization

Samples from the cast alloys were prepared using metallographic techniques adapted for magnesium alloys. Successive grinding with 600, 800, 1000, and 2000 SiC grit paper was carried out using water as coolant and ethyl alcohol as cleaning agent between grinding steps. The samples were polished with 0.25 µm diamond paste and immersed in the diamond coolant solution for a few minutes to avoid oxidation. The samples were then washed with distilled water followed by ethyl alcohol and dried with warm flowing air. For microstructure examinations by optical and scanning electron microscopes; the as cast samples were electrolytically polished and etched in a solution containing 625 ml ethanol (95%) and 375 ml phosphoric acid (85%) under cell volt of 1.5-2.5 V using steel plate as cathode. The sample was used as anode and stainless steel plate as cathode. A ZEISS Axionert optical microscope was used for microstructure examinations, whereas QUANTAFEG 250 scanning electron microscope equipped with EDX Geneses analyzer was used for microstructure investigations, phase analysis, surface morphology of corroded surfaces and surface and cross section morphology of MAO and HA coated samples.

2.3. Corrosion Tests

2.3.1. Immersion tests (hydrogen evolution method)

Simulated Body Fluid (SBF) was used as the test solution for all corrosion tests (Table 2). Tests were carried out at room temperature and pH 7.9. Corrosion rates were calculated using hydrogen gas evolution method. An ideal device, easy and simple to operate was set up, Fig.1. Disc specimens of 1.2 cm diameter were immersed in a 500-600 ml beaker containing 450 ml of the test solution, prepared using distilled water and analytical grade chemicals. A funnel was placed over the specimen to ensure the collection of all the hydrogen from the specimen surface as well as from any undermined metal particles at the bottom of the beaker. A 50 ml burette initially full of test solution was mounted over the funnel. The beakers were tightly covered to avoid solution evaporation. The volume of hydrogen gas evolved was easily measured by reading the position of the test solution levels in the burette. Test duration was 170 h and monitored every 24 h. The measured hydrogen volume can be easily converted into g moles using the ideal gas law. Simply assuming that the number of moles of the evolved hydrogen is equal to the number of moles of the dissolved magnesium, weight loss rate of the specimen can be calculated.

2.3.2 Electrochemical tests (potentiodynamic polarization test)

Electrochemical tests were carried out in a three electrode cell using a platinum electrode as the counter electrode, Ag/AgCl electrode as the reference electrode and the tested specimen as the working electrode. The working electrode (tested specimen) was immersed in the SBF testing solution for half an hour at room temperature before carrying out the test in order to attain a steady state corrosion potential (E_{corr}). Tests were performed using a potentiostat (Auto Lab PG Stat 30 Corrosion Measurement System). Potentiodynamic scan was carried out starting at -0.3 up to 1.0 V with respect to free corrosion potential E_{corr} at a scan rate of 1 mVs^{-1}.

2.4. Surface Coating Investigation

2.4.1. Micro-arc oxidation treatment

Ceramic oxide coating was prepared on the magnesium alloys using an alternating current (10 A, 100 V and 50 Hz) micro-arc discharge in a specific electrolyte composed of 15 g/l sodium silicate and 5 g/l potassium hydroxide under temperature controlled below 50 °C for about 2 min. Discs of 1.5 mm thickness machined from the magnesium alloy bar were used as the substrate material. MAO process was carried out using a high power supply unit, a stainless steel counter electrode and a cooling system. Prior to MAO process, the specimens were successively ground with 600,800 and 1200 grit paper, followed by alumina polish (0.25 µm), then rinsed with distilled water, degreased with ethyl alcohol, dried in a cool air stream. During the early stages of the MAO treatment and on increasing voltage, the plasma appears as sparks moving across the specimen surface allowing the oxidation process to go on. The sparks become micro-arc before changing to arcs. Through this process, fast formation of thick, dense and hard ceramic layer was observed.

2.4.2. Preparation of hydroxiapatite (HA) coating

The MAO treated magnesium alloy was introduced into HA coating solution. The HA solution contained calcium nitrate (8 g/l) and sodium dihydrogen phosphate (4 g/l). The samples was immersed in the HA coating solution for 30 min under microwave radiation (800 W), followed by rinsing with distilled water and then dried at 350 °C for 3 h.

2.5. Surface Characterization

X-Ray diffraction was employed for the identification of the constituent phases in the as cast condition. Mg-Zn alloys and the phase composition of MAO and HA coatings using Bruker AXS-D8 X-ray diffractometer with Cu-Kα radiation source. The morphology and composition of uncoated and coated samples were observed under scanning electron microscope (SEM, JEOL, JSM 5410, Japan) equipped with energy dispersive spectroscopy (EDS) unit.

3. Results and Discussion

3.1. Microstructure Investigation of Mg-Zn Alloys

Fig.(2a-d) represents typical microstructures of the as-cast Mg-Zn alloys. Dendritic crystals and interdendritic second-phases are present. It is observed that, when Zn content was 1 wt% (alloy Z1), the microstructure consists only of α-Mg. The maximum solubility of Zn in magnesium was about 2 wt% at room temperature in the equilibrium state [13]. When no more than 2 wt% Zn (alloy Z2) was added, Zn was dissolved in Mg matrix as solid solution and small amount of (Mg,Zn) containing phases precipitated from matrix. When Zn content was more than 2 wt.% (alloys Z3, Z4), the microstructure obviously changed, more second phases having small particles morphology were precipitated. During solidification process of of Mg-Zn alloys, these (Mg,Zn) containing phases precipitated at 340 °C by eutectic reaction:

$$L \text{ -------- } \alpha Mg + MgZn$$

On the other hand increasing Zn content has resulted in a reduction in the grain size. This indicates that the addition of Zn element can significantly refine the grain size. It is generally accepted that finer second phase has better refinement effect on the grain size than solid solution [14]. Therefore, the grain size decreases remarkably when Zn content increases up to 3 wt.%, Fig. (3C). For better degradation properties and biocompatibility, the impurity content in Mg-Zn alloys must be kept very low [15]. This is in agreement with our results as indicated in Table 1.

The microstructural observations were confirmed by XRD results as shown in Fig.(3a). XRD analyses are used to determine the existing of intermetallic phases in the Mg-Zn alloys. There is only diffraction peaks of α-Mg phase in Z1 alloy. As Zn concentration increases, diffraction peaks of $MgZn_2$ phase's pattern are detected in Z3 and Z4 alloys. On the other hand, the scan map of Z2 and Z4 proves that segregation of these elements are observed at the grain boundaries, Fig.(3b,c). At the same time, the optical microstructures of Mg-Zn alloys are confirmed by the SEM micrographs as shown in Fig.(4). The (Mg,Zn) containing phases have the strip, rod-like, and elliptical shape. The amounts of these phases are increased by increasing Zn content, Fig. 4(b,d). Meanwhile; continuous and discontinuous lamellar eutectic structures were observed in the as cast microstructure. The thickness of the lamellar structure appears to have increased significantly with increasing Zn content at the grain boundaries. These eutectic structures are coarse and mostly distributed in the grain boundaries and less in the areas of inter-dendrite, Fig.(4d). The EDS results of the second phases in Z2 and Z4 alloys are represented in Fig.(5). High Zn concentration was found at the grain boundaries and increased with Zn content.

3.2. Corrosion Investigation of Mg-Zn Alloys

3.2.1. Hydrogen evolution test

Immersion test depends on magnesium dissolution. It is well established that hydrogen evolution method is the best approach in this respect [16], where it has been demonstrated theoretically and experimentally that the amount of hydrogen collected is equal to the amount of magnesium dissolved. The degradation rates of the investigated alloys are shown in Fig.(6). Corrosion rates in mm/y after 170 h immersion are represented in histogram Fig.(7). Mg-Zn alloys Z1, Z2, Z3 have shown very low corrosion rates (0.025 mm/y) through the total immersion period, whereas Z4 has shown an almost linear increase up to the 170 h immersion. This was mainly attributed to precipitation of second cathodic phases, difference in grain size, and absence of continuous protective film as formed on Mg- 1,2,3 wt% Zn alloys.

Surface morphologies of samples of Mg–Zn alloys soaked in SBF for 170 h are shown in Fig.(8). For these alloys, pitting corrosion is almost insignificant on Z1 and Z2. It started to show as shallow laterally spread pits on Z3, whereas Z4 is the most severely attacked sample in this group. This is in conformity with the hydrogen evolution test results shown before and could be related to the fine microstructure of Z2 and Z3, compared with Z1 and Z4 (Fig.2). Also, the presence of precipitates or the cathodic phases in Z3, Z4 led to selective attack of the matrix around these phases and its peeling off the surface forming pits which grow in size and agglomerate into irregular array from which dramatic evolution of hydrogen takes place [17]. Examination of specimens Z1 and Z4 was carried out using SEM equipped with EDS. Specimen Z1 has shown almost intact surface with few shallow cracks due to hydrogen evolution at low rate; peaks of P & Ca were detected indicating the formation of protective calcium phosphate layer, Figs.(9 a,b). On the other hand, specimen Z4 showed more pronounced pitting attack spreading on the surface, where peaks of Mg rather than Ca or P were detected (Fig.9

c,d). Relatively small dispersed areas were found to have Ca and P peaks, indicating that the surface of the corroded specimen is not properly protected. The deep cracks observed on this specimen could be attributed to strong hydrogen evolution and dehydration of the corrosion products in the corroded layer after drying in warm air and the SEM vacuum chamber.

3.2.2. Potentiodynamic behavior

Potentiodynamic polarization curves of Mg-Zn alloys in SBF solution are given in Fig.(10). The highest corrosion potential (E_{corr}) was for alloy Z3 (- 1.39 V), followed by Z4 (- 1.44 V) then, Z2 (-1.48 V) and finally Z1 (-1.53 V). The variation range is about 140 mV. It can be noticed that increasing Zn content has shifted E_{corr} to more noble potential. The limiting current (I_L) is almost the same for all alloys. Passivation of the alloys or the formation of protective layer is not evident. Generally, cathodic polarization curves are assumed to represent the cathodic reaction (hydrogen evolution) through water reduction, while anodic polarization curves represent dissolution of magnesium matrix or α-phase. It can be noticed that the highest cathodic current was obtained for Z3, followed by Z4 then Z1 and finally Z2. It can be concluded that cathodic reaction was kinetically more difficult on Z2, Z1, Z3 then Z4. Consequently, the degradation rates of Z1, Z2 and Z3 were slower than that of Z4. This is almost in conformity with the results obtained for hydrogen evolution test, where Z4 has the highest corrosion rate.

3.3. Micro-arc oxidation/hydroxiapatite surface coating morphology

Surface morphology of the MAO treated magnesium alloys are shown in Fig. (11a,b). A porous ceramic oxide film was formed throughout the surface with a layer thickness of 10 µm (Fig.11e). The MAO coating is composed of a dense inner layer and a porous outer layer. Round pores of 2-5 µm diameters are shown in the porous outer layer, but they do not penetrate the dense inner layer. After HA treatment (Fig.11c,d), the large pores on the MAO treated alloys became smaller (2µm) and some of them were sealed due to the formation of fine dendritic structure of HA. After MAO/HA treatment, coating is not dense enough and many pores were found on the surface. The pores are likely to be beneficial for the infiltration of new bone tissues into the implants and accelerating the healing of the damaged bones [18,19]. The fine dendritic structure of the HA coating was helpful for bone growth.

The formation of HA observed in Fig. (11c & d) was confirmed by EDS composition analysis, as shown in Fig.(11f). Ca and P were detected in the porous MAO layer. Carbon element (C) was detected in HA coating possibly caused by the dissolution of CO_2 from surrounding atmosphere. CO_3^{2-} might substitute the PO_4^{3-} in the apatite, producing a coating that has a similar composition with the biological apatite from natural bone mineral which is beneficial to the biocompatibility [18].

The XRD pattern Fig.(12) has shown that the MAO ceramic coating is mainly composed of MgO phase and Mg_2SiO_4. In aqueous solution of MAO electrolyte, the sodium silicate is easy to be hydrolyzed to $Si(OH)_4$. Under condition of high temperature resulting from discharge during the micro-arc oxidation process, $Si(OH)_4$ is dehydrated to SiO_2 through the following reactions [20]:

$$SiO_4^{4-} + 4\,H_2O \rightarrow Si(OH)_4 + 4\,OH^-$$
$$Si(OH)_4 + Si(OH)_4 + \ldots. \rightarrow xSiO_2.yH_2O$$
$$xSiO_2.yH_2O \rightarrow xSiO_2 + yH_2O$$

Some SiO_2 and MgO transforms into Mg_2SiO_4.

$$SiO_2 + 2\,MgO \rightarrow Mg_2SiO_4$$

3.4. Corrosion Behavior of Coated Mg-Zn Alloys

Potentiodynamic polarization curves of the four uncoated magnesium alloys (Z1, Z2, Z3 and Z4), two MAO treated samples and four MAO/HA coated samples are shown in Figs. (10,12 & 14), respectively. The corresponding electrochemical parameters, including corrosion potential (E_{corr}), corrosion current density (I_{corr}) and corrosion rate (CR) are listed in Table(5). The highest corrosion resistance sample is the one shows the lowest corrosion current and corrosion rate. The corrosion resistance of the uncoated alloys decreases in the following order: Z2 > Z3> Z1 > Z4, whereas in case of MAO/HA coated alloys the order has changed with Z1 having the best performance; Z1 > Z2> Z3 > Z4. Compared to the uncoated samples, the MAO/HA coated samples show a marked increase in corrosion resistance, especially in the case of Z1 alloy where corrosion resistance increased by 20 times.

The effect of MAO/HA coating was related to relative conversion of MgO into $Mg(OH)_2$ leading to blocking of pores due to volume expansion. Further expansion with time results in breaking down of pores and cracking of micro-arc oxidation film, providing another pathway for penetration of chloride ions and corrosion of the substrate alloys [21,22].

4. Conclusions

Zn was selected in this work to develop some biodegradable magnesium alloys for biomedical applications due to its good biocompatibility. Microstructures characterizations of Mg-Zn (1-4wt.%) were investigated. Coating effect was also investigated. Corrosion behavior of the alloys was thoroughly studied. From the obtained results, the following conclusions could be drawn:

1. Mixtures of CO_2-Air combined with 0.3-0.5% SF_6 have been successfully used for melt protection in casting operations of Mg-Zn alloys, thus, essentially eliminating the problems due to flux inclusions. At the same time, SF_6 being a source of both sulfur and fluorine provides a very effective barrier.
1. The microstructure of the as-cast Mg-Zn alloys is composed of α-Mg and secondary phases which precipitated along the grain boundaries. In addition, the grain size of Mg decreases with increasing Zn content.
2. The X-ray diffraction pattern showed that the predominant phases of Mg-Zn alloys were α-Mg and the second $MgZn_2$ phases. It was found that up to 2 wt.% Zn, Zn is completely dissolved in the α-Mg matrix. With increasing Zn content, the second $MgZn_2$ phase is formed.
3. SEM micrographs and EDS analysis of Mg-Zn alloys reveal the presence of primary α dendrites and one or more second phases at the grain boundaries and in the inter-dendritic regions (Mg,Zn) having strip and rod-like shapes.
4. Hydrogen evolution, as the most reliable method to evaluate the corrosion rates of magnesium alloys, revealed that Mg- 1,2,3 wt.% Zn have almost the same corrosion rates (0.025 mmy), whereas Mg- 4 wt% Zn has a higher corrosion rate.
5. Potentiodynamic test is in conformity with the results obtained by hydrogen evolution method.
6. Through HA coating on MAO treated magnesium alloys, a dense and compact layer is formed on the surface of magnesium alloys by which its surface property has largely improved.

5. References

1. Song GL (2007) Control of biodegradation of biocompatible magnesium alloys. Corros Sci 49:1696-1701.
2. Witte F, Fischer V and Nellesen J (2006) In vitro and in vivo corrosion measurements of magnesium alloys. Biomater 27:1013-1018.
3. Staiger MP, Pietak AM, Huadmai J and Dias GJ (2006) Magnesium and its alloys as orthopedic biomaterials: a review. Biomater 27:1728-1734.
4. Song GL and Song SZ (2006) Corrosion behavior of pure magnesium in a simulated body fluid. Acta Physico-Chimica Sinica 22:1222-1226.
5. Hamid H and Coltart J. Magnesium (2007) An essential nutrient for a good biomaterial. MG Gill Journal of Medicine 10:105-111.
6. Zeng RC, Dietzel W, Witte F, Hort N and Blawert C (2008) Progress and Challenge for Magnesium Alloys as Biomaterials. Adv. Eng. Mater 10:B3-B14.
7. Wang H, Estrin Y, Fu HM, Song GL and Zuberova Z (2007). *The effect of pre-processing and grain structure on the bio-corrosion and fatigue resistance of magnesium alloy AZ31.* Adv. Eng. Mater 9:967-972.
8. Abd El Hallem SM, Ghayad IM, Eiasa M, Nassif N, Shoeib MA and Soliman H (2014) Effect of Ultrasonic and Mechanical Vibration on the Corrosion Behavior of Mg-3Zn-0.8Ca Biodegradable Alloy. Int J Electrochem Sci 9:2005-1015.
9. Witte F, Hort N, Vogt C, Cohen S, Kainer K, Willumeit R and Feyerabend F (2008) Degradable biomaterials based on magnesium corrosion. Current Opinion Solid State Mater Sci 12: 63-72.
10. Südholz AD, Birbillis N, Bettles CJ and Gibson MA (2009) Corrosion behavior of Mg-alloy AZ91E with a typical alloying additions. J Alloys Compd 47:109-115.
11. Roberts CS. Magnesium and its Alloys, New York: Wiley (1960) Wily Series on the Science and Technology of Materials.
12. Girgis NN and Ghayad IM (2013) Corrosion Protection and Surface Treatment of Magnesium Alloys Used for Orthopedic Application. Advances in Materials Science and Engineering. Doi:10.1155/2013/532896.
13. Nayeb-Hashemi AA and Clark JB (1988) Phase Diagrams of Binary Magnesium Alloys, Metals Park, Ohio; ASM, p. 344.
14. Dong-song Y., Er-lin Z., and Song-yan Z (2008) Effect of Zn on mechanical property and corrosion property of extruded Mg-Zn-Mn alloy. Trans Nonferrous Met Soc China 18:763-768.
15. Murray RW and Hillis JE (1990) SAE Technical Paper Series #900 791, Detroit, USA.
16. kubok K, Litynska-Dobrzynska L, Wojewoda-Budka J, Goral A and Debski A (2008) The development of a new grain refiner for magnesium alloys using the edge-to-edge model. J Alloys Comp 456:390-394.
17. Huan ZG, Leeflang MA, Zhou J, Fratile-Apachitei LE and Duszczy KJ (2010) In vitro degradation behavior and cytocompatibility of Mg–Zn–Zr alloys. J Mater Sci Mater Med 21:2623-2635.
18. Song G, Atrens A, Vu X and Zhang B (1998) Corrosion behavior of AZ21, AZ501 and. AZ91 in sodium

chloride. Corros Sci 40 :1769-1791.
19. Wen CL, Guan SK, Peng L, Ren CX, Wang X and Hu ZH (2009) Characterization and degradation behavior of AZ31 alloy surface modified by bone-like hydroxyapatite for implant applications. App Surf Sci 255:6433-6438.
20. Xia SJ, Yue R, Rateick JRG and Birss VI (2004) Electrochemical Studies of AC/DC Anodized Mg Alloy in NaCl Solution. J Electrochem Soc 251:B179-B187.
21. Suhanec W and Yoshimura M (1998) Processing and properties of hydroxyapatite-based biomaterials for use as hard tissue replacement implant. J Mater Res 13:94-117.
22. Liu L, Yang P, Su C, Guo H and An M (2013) Microstructure and corrosion behavior of micro-arc oxidation film on magnesium alloy. Int J Electrochem Sci 8:6077-6084.

Table 1: Chemical compositions of the as cast Mg alloys

Alloy	Symbol	Zn	Al	Si	Fe	Mg
Mg-1Zn	Z1	1.2	< 0.3	0.3	0.00	Bal.
Mg-2Zn	Z2	2.1	< 0.3	0.3	0.01	Bal.
Mg- 3Zn	Z3	3.16	< 0.3	0.3	0.01	Bal.
Mg- 4Zn	Z4	4.11	< 0.3	0.3	0.03	Bal.

Table 2: Chemical composition of SBF

Chemicals	NaCl	KCl	$CaCl_2$	$NaHCO_3$	$C_6H_6O_6$	$MgSO_4.7H_2O$	$KH_2PO_4.H_2O$	$Na_2HPO_4.7H_2O$
Composition, g/l	8.8	0.4	0.14	0.35	1	0.2	0.1	0.06

Table 3: Corrosion parameters of uncoated, MAO and MAO/HA coated samples

Sample	**E_{corr} /V**	**I_{corr}/ Acm^{-2}**	**CR/mm yr^{-1}**	**CR Factor (times)**
Z1-uncoated	-1.53	8.965×10^{-6}	0.1989	-
Z1- MAO Coated	-1.385	3.639×10^{-6}	0.164	1.25
Z1- MAO/HA Coated	-1.422	2.259×10^{-7}	0.0102	20
Z2-uncoated	-1.57	5.35×10^{-6}	0.122	-
Z2- MAO Coated	-1.587	7.22×10^{-7}	0.0326	3.7
Z2- MAO/HA Coated	-1.473	3.38×10^{-7}	0.0153	8
Z3-uncoated	-1.56	5.66×10^{-6}	0.128	-
Z3-MAO/HA Coated	-1.47	7.323×10^{-7}	0.031	4
Z4-uncoated	-1.44	1.41×10^{-5}	0.322	-
Z4-MAO/HA Coated	-1.33	1.713×10^{-6}	0.0774	4

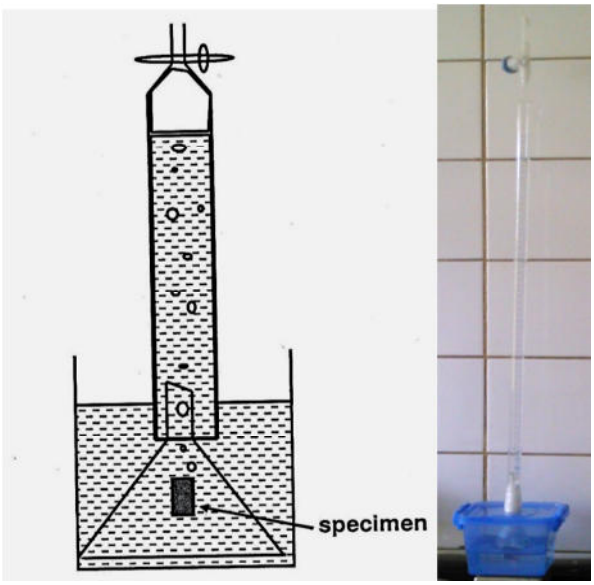

Fig. 1: Schematic and implemented device for hydrogen evolution test

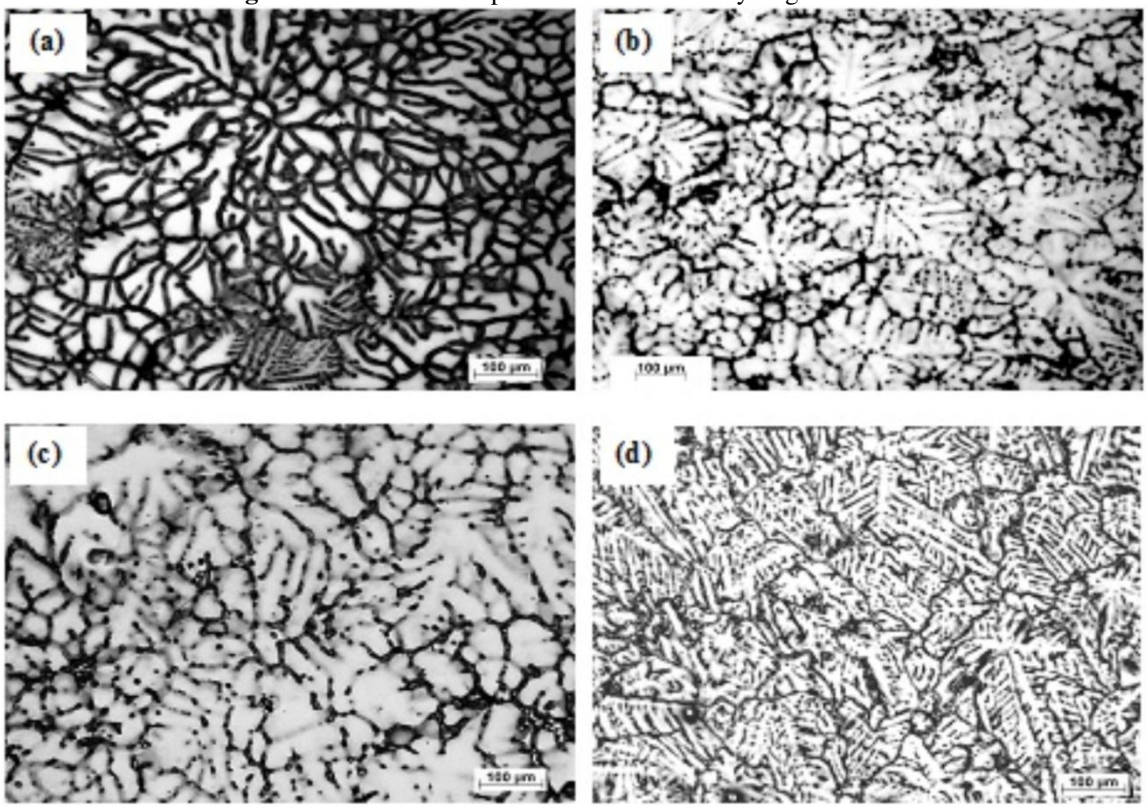

Fig. 2: Optical Microstructures of as-cast Mg-Zn alloys (a) Z1, (b) Z2, (c) Z3, and (d) Z4

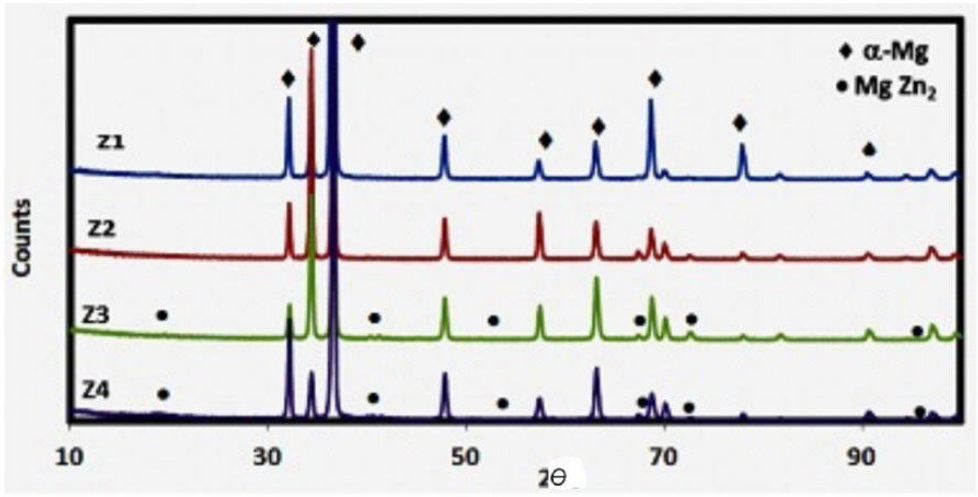

(a)

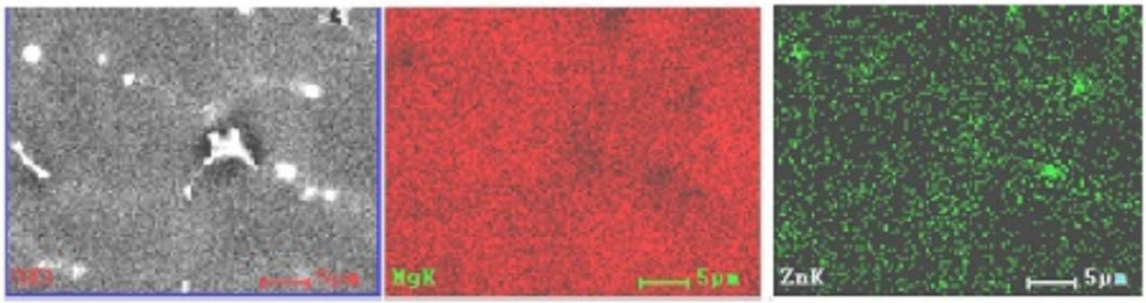

(b)

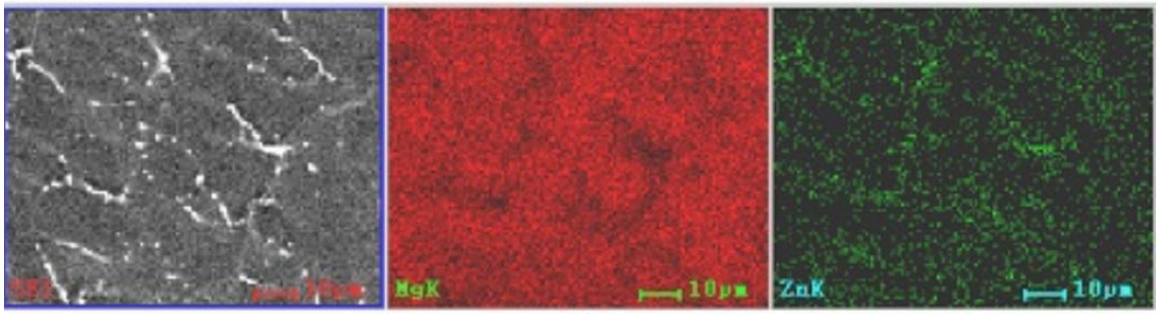

(c)

Fig. 3: (a) XRD of as-Cast Mg-Zn alloys, (b) Map of Z2, (c) Map of Z4

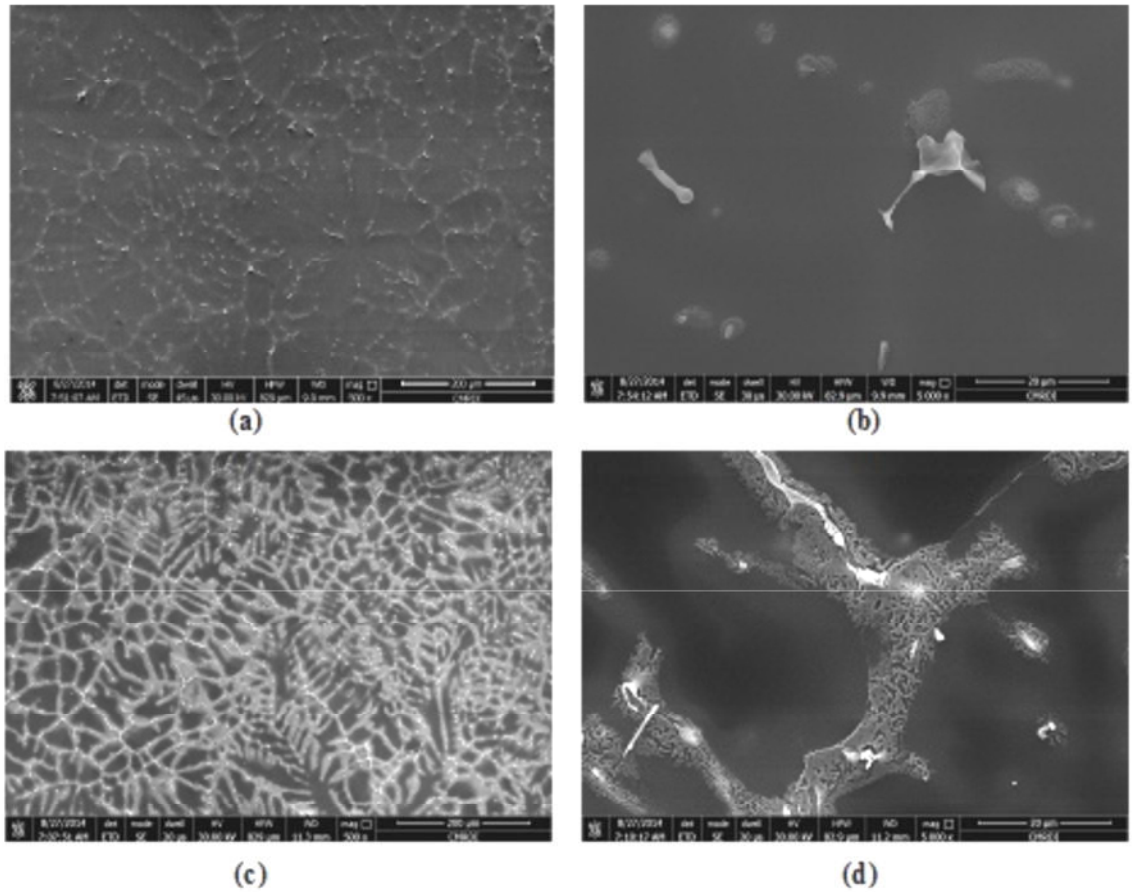

Fig. 4: SEM micrographs of as cast Mg-Zn alloys; (a) Z1, (b) Z2, and (c) Z3, (d) Z4

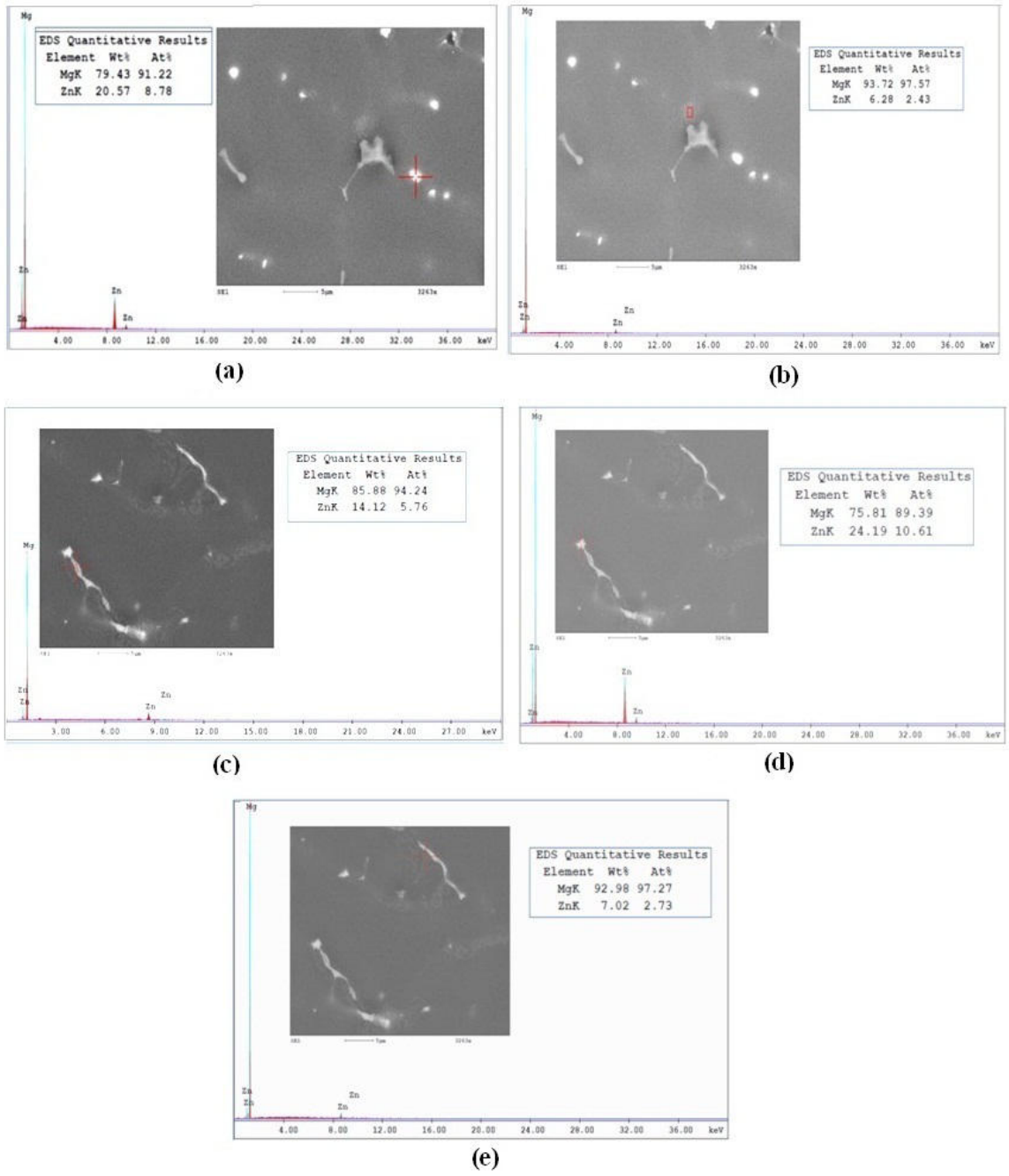

Fig. 5: EDS of precipitates on Z2 alloy (a,b) and Z4 alloy (c,d,e)

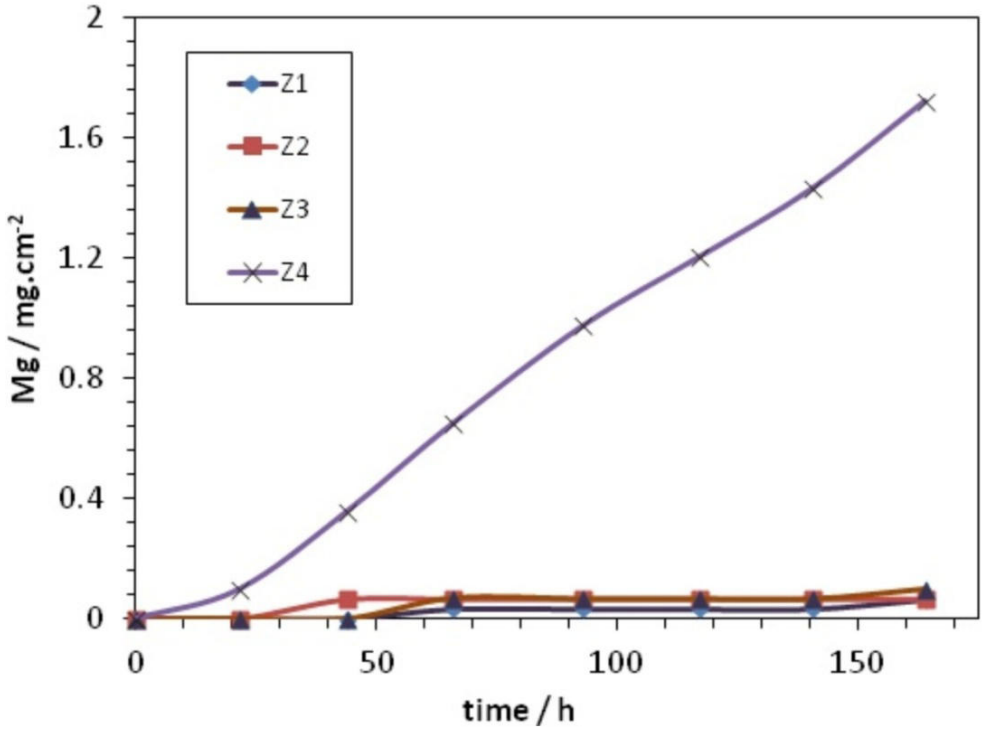

Fig. 6: Degradation rates of Mg-Zn alloys calculated after seven days immersion in SBF

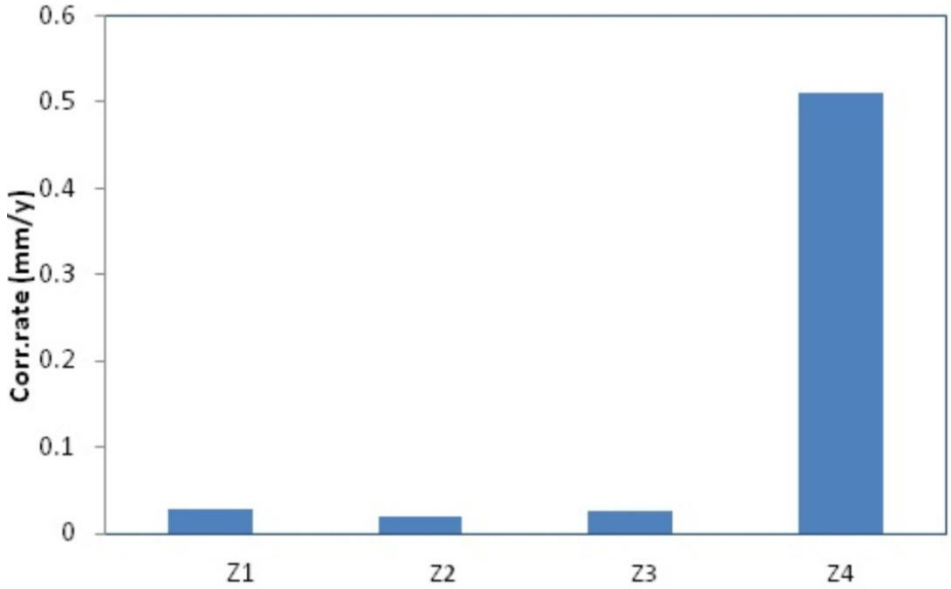

Fig. 7: Histogram of corrosion rates of the Mg-Zn alloys calculated after 7 days immersion in SBF solution

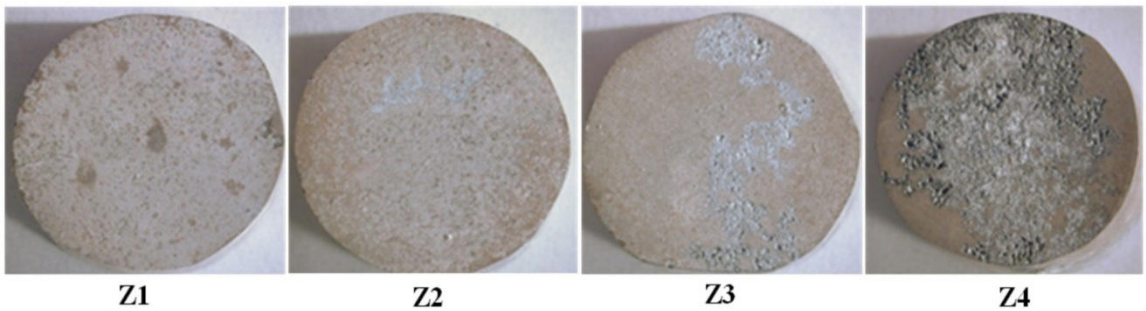

Fig. 8: Macrographs of the tested Mg-XZn alloys

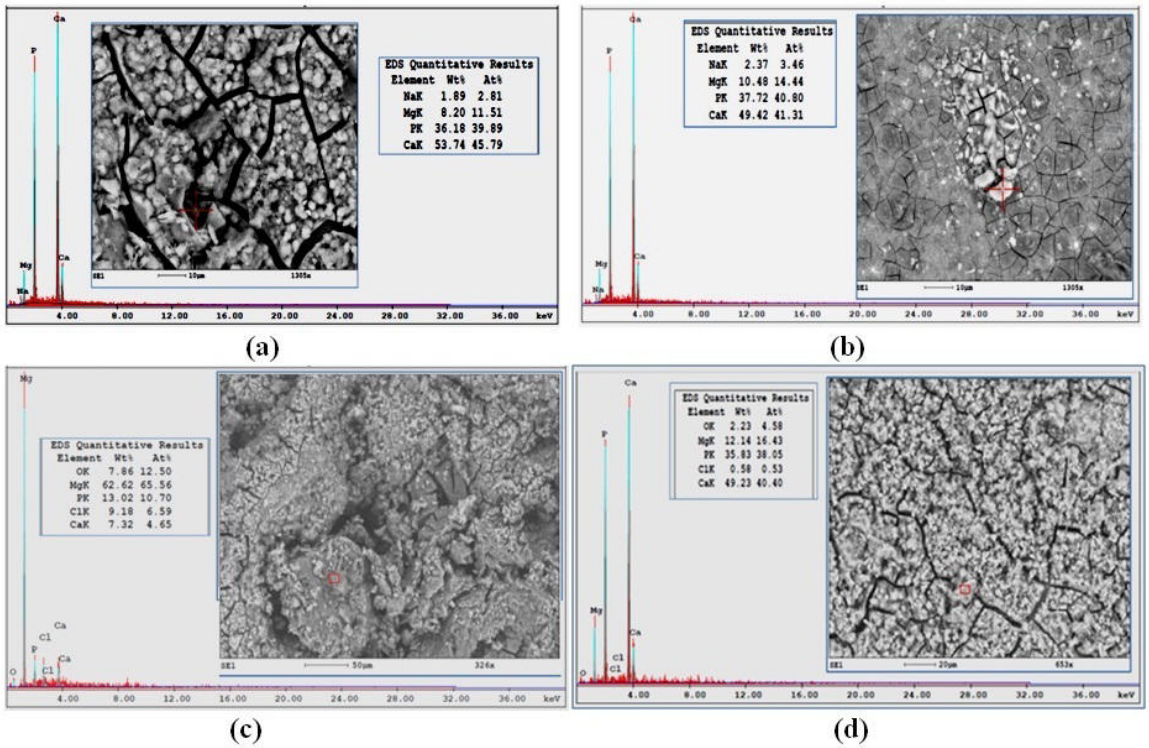

Fig. 9: SEM and EDS of Z1 and Z4 alloys; (a) EDS on Z1 alloy surface, (b) EDS on Z1 deposits, (c) EDS on Z4 alloy surface, (d) EDS on Z4 deposits

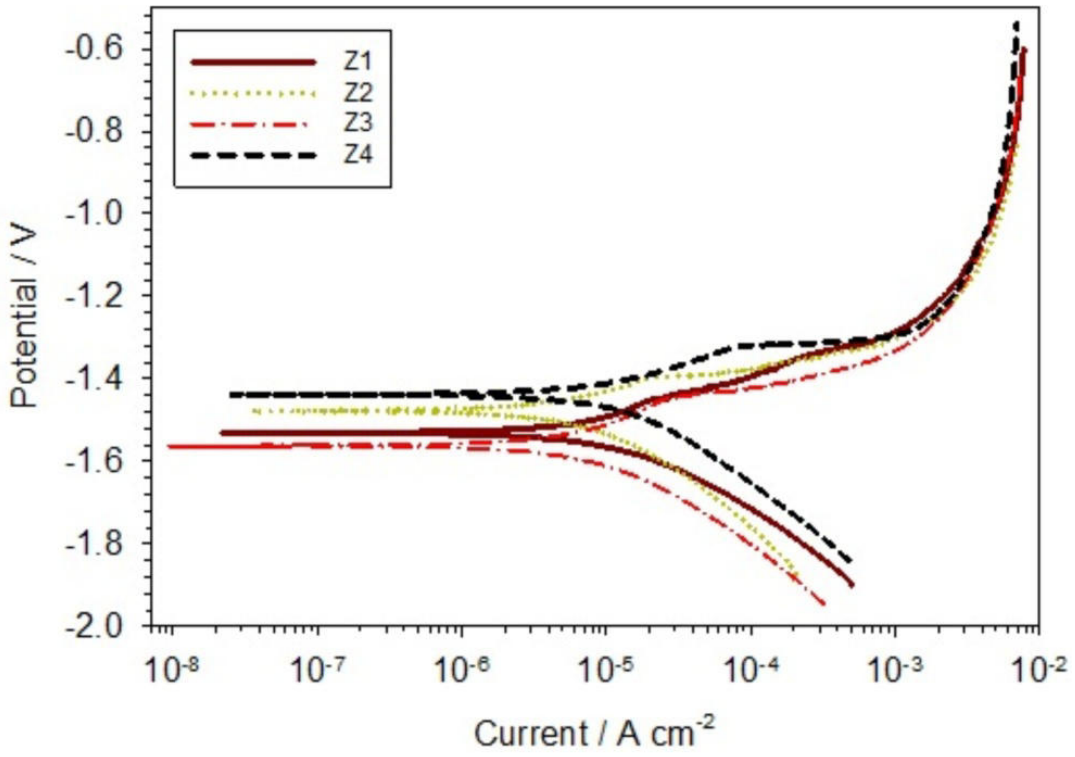

Fig. 10: Potentiodynamic behavior of the investigated (Mg-Zn) alloys

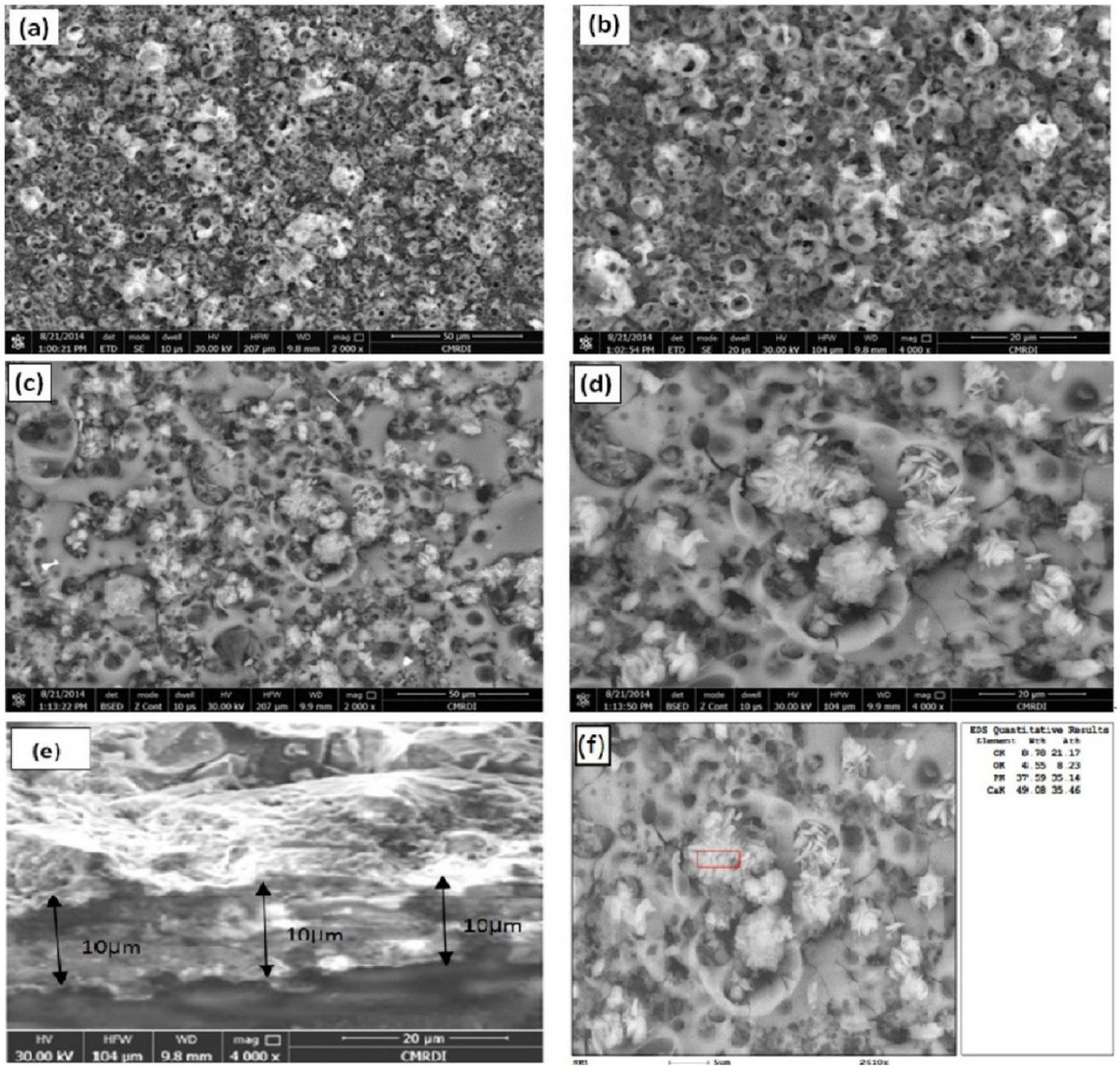

Fig. 11: SEM morphology of MAO & MAO/HA coated Z1 alloy; (a, b) MAO, (c, d) MAO/HA, (e) Cross section MAO/HA coat. Image (f) represents the EDS analysis of HA

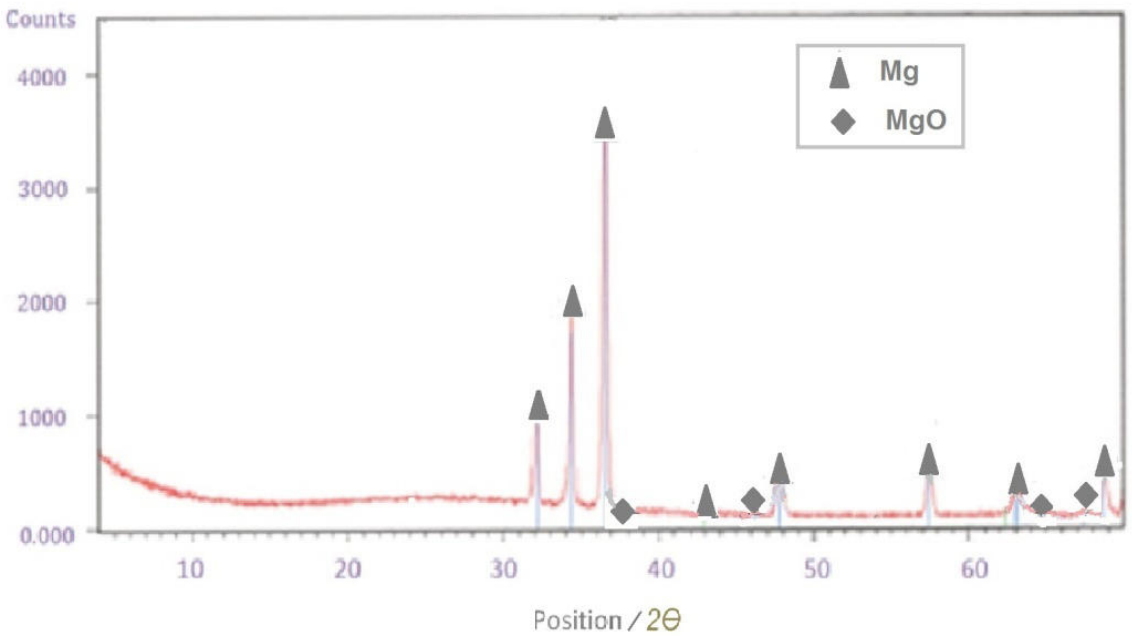

Fig. 12: XRD pattern of MAO coating on Z1 alloy

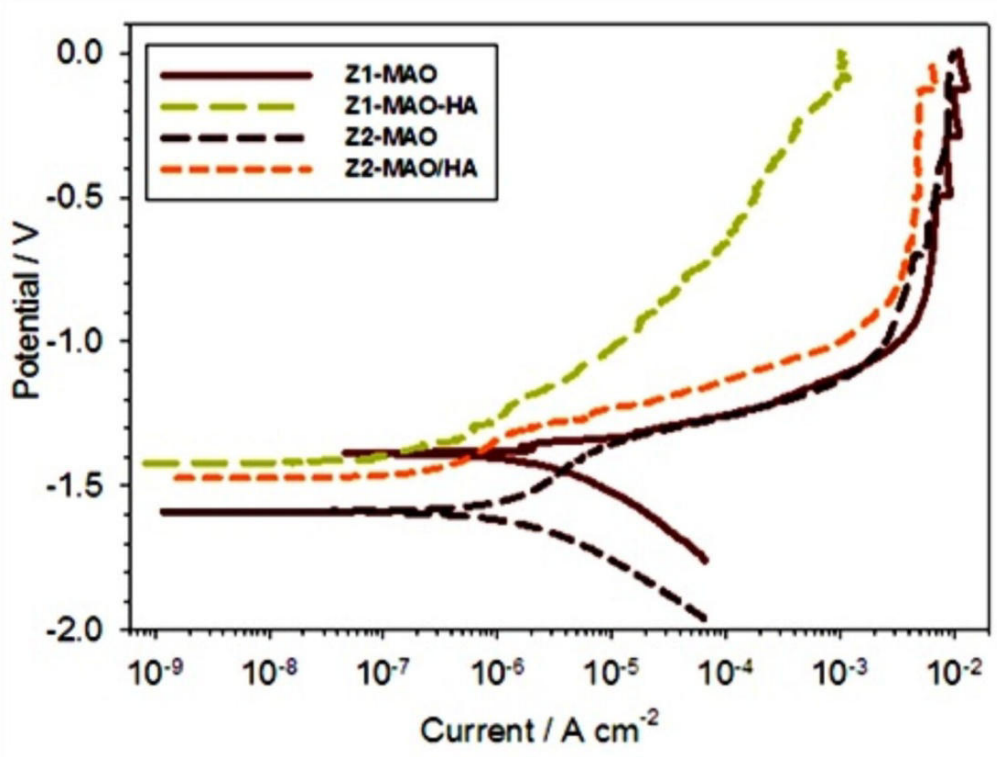

Fig. 13: Potentiodynamic polarization curves of MAO and MAO/HA coated Z1 and Z2 samples

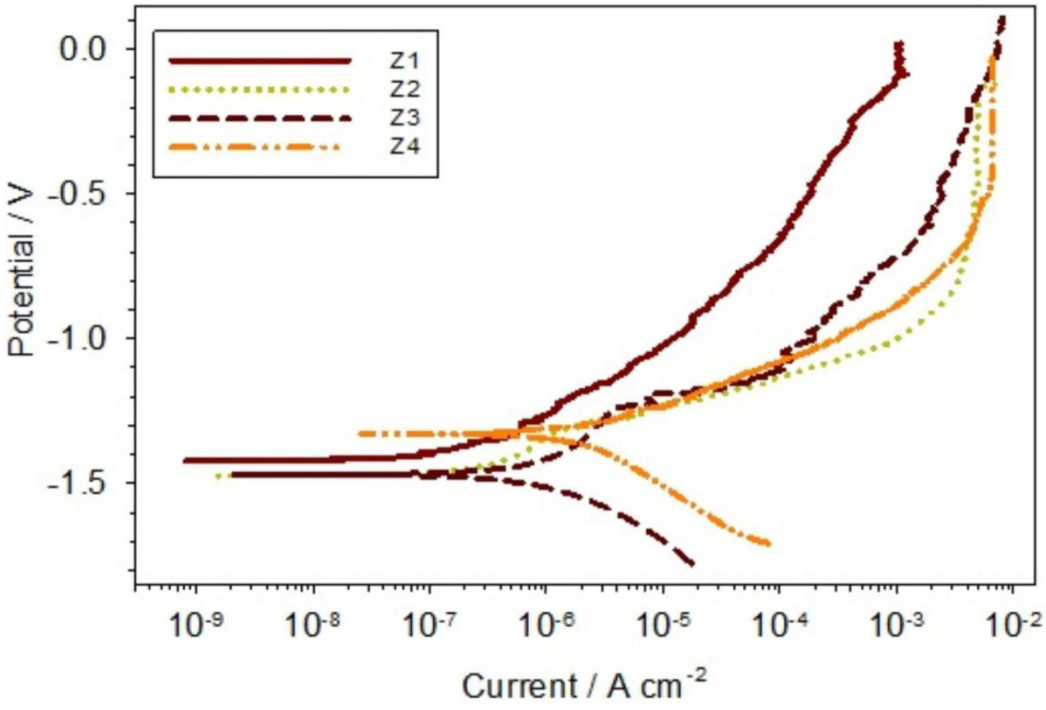

Fig 14: Potentiodynamic polarization curves of MAO/HA coated Mg-Zn samples

The IISTE is a pioneer in the Open-Access hosting service and academic event management. The aim of the firm is Accelerating Global Knowledge Sharing.

More information about the firm can be found on the homepage:
http://www.iiste.org

CALL FOR JOURNAL PAPERS

There are more than 30 peer-reviewed academic journals hosted under the hosting platform.

Prospective authors of journals can find the submission instruction on the following page: http://www.iiste.org/journals/ All the journals articles are available online to the readers all over the world without financial, legal, or technical barriers other than those inseparable from gaining access to the internet itself. Paper version of the journals is also available upon request of readers and authors.

MORE RESOURCES

Book publication information: http://www.iiste.org/book/

Academic conference: http://www.iiste.org/conference/upcoming-conferences-call-for-paper/

IISTE Knowledge Sharing Partners

EBSCO, Index Copernicus, Ulrich's Periodicals Directory, JournalTOCS, PKP Open Archives Harvester, Bielefeld Academic Search Engine, Elektronische Zeitschriftenbibliothek EZB, Open J-Gate, OCLC WorldCat, Universe Digtial Library , NewJour, Google Scholar